



Cite this: *Phys. Chem. Chem. Phys.*,
2015, 17, 11732

A new potential energy surface for the ground electronic state of the LiH₂ system, and dynamics studies on the H(²S) + LiH(X¹Σ⁺) → Li(²S) + H₂(X¹Σ_g⁺) reaction

Jiuchuang Yuan,[†] Di He[†] and Maodu Chen*

A new global potential energy surface (PES) is obtained for the ground electronic state of the LiH₂ system based on high-level energies. The energy points are calculated at the multireference configuration interaction level with aug-cc-pVXZ (X = Q, 5) basis sets, and these energies are extrapolated to the complete basis set limit. The neural network method and hierarchical construction scheme are applied in the fitting process and the root mean square error of the fitting result is very small (0.004 eV). The dissociation energies and equilibrium distances for LiH(X¹Σ⁺) and H₂(X¹Σ_g⁺) obtained from the new PES are in good agreement with the experimental data. On the new PES, time-dependent wave packet studies for the H(²S) + LiH(X¹Σ⁺) → Li(²S) + H₂(X¹Σ_g⁺) reaction have been carried out. In this reaction, no threshold is found due to the absence of an energy barrier on the minimum energy path. The calculated integral cross sections are high at low collision energy and will decrease with the increase of the collision energy. The product molecule H₂ tends to be forward scattering due to direct reactive collisions, which becomes more evident at higher collision energies.

Received 18th November 2014,
Accepted 30th March 2015

DOI: 10.1039/c4cp05352d

www.rsc.org/pccp

1 Introduction

In recent years, lithium chemistry has received much attention due to its important role in the evolution of the primordial universe.^{1–9} The formation and depletion of LiH molecules play an important part in galactic lithium production and stellar evolution.^{2,3} The H + LiH reaction is considered as an important pathway of LiH depletion.^{4,5} Furthermore, the physical significance of the reactive system also makes it attractive. The LiH₂ system is the simplest of the alkali metal–dihydrogen partners containing only five electrons, which makes it a good research subject for nonadiabatic transition study. For these reasons, a flurry of studies have been carried out on the LiH₂ chemical system during the past decade.^{10–29}

To study the reaction dynamics, it is necessary to construct the potential energy surface (PES), which describes the interactions of the molecular system. In the past decade, several three-dimensional ground-state (²A') PESs of the LiH₂ system^{10,13,17,18,26} have been constructed to investigate the dynamics of the reactive processes.

The first full three-dimensional PES was developed by Dunne, Murrell, and Jemmer (DMJ)¹⁰ using an *ab initio* configuration interaction (CI) method and spectroscopic data. The energy

data of approximately 300 randomly generated configurations of LiH₂ were sampled, and the augmented correlation-consistent polarized valence double zeta basis set (aug-cc-pVDZ) was employed in the calculation. The PES was fitted to a standard many-body form and the two-body parts were taken as extended Rydberg potentials. The root mean square error (RMSE) of the fitting result was 0.09 eV, and the maximum error was 0.36 eV. In 2003, Kim *et al.*¹³ calculated energy data at the multireference configuration interaction (MRCI) level with a complete active space self-consistent field (CASSCF) reference wave function. About 7000 points were selected, and the interpolant moving least squares (IMLS)/Shepard scheme was used for the interpolation of the PES. With the increase in computing power, energy points with higher precision were calculated to construct the PES of this system. In 2009, Wernli *et al.*¹⁷ reported a global three-dimensional PES (Wernli PES), which was fitted by large-scale calculated energy data (23 300 points) in an analytic form (modified Aguado–Paniagua form). The energy data was calculated at the MRCI level with a CASSCF reference wave function, and correlation-consistent polarized valence quadrupole zeta (cc-pVQZ) basis set was employed. In the same year, Prudente *et al.*¹⁸ also structured an analytic PES (Prudente PES) to study the reaction dynamics of the H + LiH reaction. The energy data was calculated using the full CI method with the aug-cc-pVQZ basis set. Based on the energy data, the analytical PES function was obtained employing the many-body expansion, and the root

Key Laboratory of Materials Modification by Laser, Electron, and Ion Beams (Ministry of Education), School of Physics and Optoelectronic Technology, Dalian University of Technology, Dalian 116024, P. R. China. E-mail: mdchen@dut.edu.cn

[†] These authors contributed equally to this work.

mean square deviation (RMSD) was 0.064 eV. In 2011, Hsiao *et al.* constructed the PESs of the $1A'$ and $2A'$ states for the $\text{Li}(2^2\text{P}) + \text{H}_2$ reaction and carried out quasiclassical trajectory (QCT) calculations.²⁶ In the QCT calculation, the transition probability for the trajectories at the crossing seam region was assumed to be unity and the trajectories changed to the lower surface for simplicity.

In recent years, the Wernli PES¹⁷ and the Prudente PES¹⁸ were widely applied to study the reaction dynamics. The small difference between the two PESs is the early-staged energy barrier on the Prudente PES,¹⁸ which doesn't exist on the Wernli PES.¹⁷ Due to the difference, the physical pictures obtained from the two PESs were obviously different, especially at low collision energy.²⁹ Therefore, for the title reaction, a more accurate PES is needed to obtain reasonable dynamics results. In this work, we report an accurate global PES for the lowest doublet state of the LiH_2 ($2A'$) system. Normally, the quality of a PES is determined by the precision of the energy data and fitting method. For high-precision energy data, we use an expanded basis set in the calculations. To date, many fitting methods have been developed, and the most common one is many-body expansion, which is used widely to construct PESs.^{30–32} In recent years, the neural network (NN) method has received much attention as a powerful tool to construct PESs for a wide range of systems.^{33,34} For example, in 2013, a high-precision PES for the $\text{F} + \text{HD}$ reaction was constructed using the NN method, and the dynamics results calculated based on the PES were in very good agreement with experimental results.³⁵ At the end of this work, based on the new PES, the time-dependent wave packet (TDWP) calculation is carried out to study the dynamics of the $\text{H}(^2\text{S}) + \text{LiH}(X^1\Sigma^+) \rightarrow \text{Li}(^2\text{S}) + \text{H}_2(X^1\Sigma_g^+)$ reaction.

2 Potential energy surface

2.1 *Ab initio* calculations

The *ab initio* calculations have been carried out using the internally-contracted MRCI^{36,37} with a CASSCF^{38,39} reference wavefunction. The CASSCF orbitals were obtained by employing equally-weighted state-averaged calculations for the ground state $1^2A'$ and the first excited state $2^2A'$ of the LiH_2 system. Three valence electrons of the LiH_2 molecule were included in eleven active orbitals ($9a' + 2a''$). Core-valence electron correlation was recovered, including single excitations out of the doubly-occupied $\text{Li}(1s^2)$ core orbitals. In both the CASSCF and MRCI calculations, the Dunning-weighted correlation-consistent polarized core-valence quadruple- ζ and quintuple- ζ (cc-pwCVXZ, $X = \text{Q}, 5$) basis sets were employed for the Li atom. At the same time, the augmented correlation-consistent polarization valence quadruple and quintuple- ζ (aug-cc-pVXZ, $X = \text{Q}, 5$) basis sets were employed for the H atom. The Jacobi coordinates were used for generating *ab initio* energy grid points. For the reaction $\text{H} + \text{LiH} \rightarrow \text{Li} + \text{H}_2$, the reactant region was defined as $1.3 \leq R_{\text{LiH}}/a_0 \leq 20$, $0 \leq R_{\text{H-LiH}}/a_0 \leq 20$, $0 \leq \theta/\text{degrees} \leq 180$, and the product region was chosen as

$0.6 \leq R_{\text{HH}}/a_0 \leq 20$, $0 \leq R_{\text{Li-HH}}/a_0 \leq 20$, $0 \leq \theta/\text{degrees} \leq 90$. All *ab initio* calculations in the present work were performed with the MOLPRO package.⁴⁰ In this work, 12 156 *ab initio* MRCI/(WCVQZ_{Li}/AVQZ_H) points were calculated to construct the PES, and 2234 [MRCI/(WCV5Z_{Li}/AV5Z_H) MRCI/(WCVQZ_{Li}/AVQZ_H)] *ab initio* points were calculated to extrapolate the correlation energy to the complete basis set (CBS) limit to improve the precision of this PES. The CBS limit correlation energy was extrapolated using the formula:⁴¹

$$E_X^{\text{corr}} = E_\infty^{\text{corr}} + AX^{-3}, \quad (1)$$

where $X = 4$ for the WCVQZ_{Li}/AVQZ_H basis set and $X = 5$ for the WCV5Z_{Li}/AV5Z_H basis set. Then the CBS limit for the correlation energy is

$$E_\infty^{\text{corr}} = \left(E \left(\frac{\text{MRCI}}{\text{WCV5Z}_{\text{Li}}/\text{AV5Z}_{\text{H}}} \right) - E \left(\frac{\text{MRCI}}{\text{WCVQZ}_{\text{Li}}/\text{AVQZ}_{\text{H}}} \right) \right) \times \frac{4^{-3}}{4^{-3} - 5^{-3}}. \quad (2)$$

The Hartree-Fock (HF) energy was not extrapolated to the CBS because there is almost no difference in the HF energy between the WCV5Z_{Li}/AV5Z_H and WCVQZ_{Li}/AVQZ_H levels for $\text{LiH}_2(1^2A)$. For the diatomic potentials of H_2 and LiH , 54 and 92 points were calculated at the MRCI/CBS level, respectively, using the method mentioned above.

2.2 Fitting the potential energy surface

The total analytical expression of the global surface is presented as

$$V_{\text{total}}(\mathbf{R}) = \sum_n V_n^{(2)}(R_n) + V_{\text{LiHH}}^{(3)}(\mathbf{R}) \cdot f(\mathbf{R}), \quad (3)$$

where \mathbf{R} is a collective variable of all the internuclear distances. $V_n^{(2)}$ ($n = \text{HH}, \text{LiH}_a, \text{LiH}_b$) is the diatomic potential, and R_n is the bond length of the relevant diatomic. $V_{\text{LiHH}}^{(3)}$ is the three-body term. $f(\mathbf{R})$ is the switch function that is used in order to have a well-described PES in the asymptotic region, and it can be written as follows:

$$f(\mathbf{R}) = \prod_n \left(1 - \frac{1}{2} \left(1 + \tanh \left(\frac{R_n - R_d}{R_w} \right) \right) \right), \quad (4)$$

where $n = \text{HH}, \text{LiH}_a, \text{LiH}_b$. R_d is the position to switch and R_w is the switch strength constant.

The NN method⁴² was used to build both the two-body and the three-body potential energy terms. The idea of NN is inspired by the central nervous system of an animal. In NN the basic unit is a neuron, which receives input signals and emits an output signal at a synapse. For a neuron, the output signal y can be written as

$$y = \phi \left(\sum_{i=1}^N w_i x_i + b \right), \quad (5)$$

where x_i ($i = 1, \dots, N$) is the input signal, w_i is the connection weight, b is a bias, and ϕ is a transfer function. To date, there

are many NN types developed for various purposes, and the most common one is the feed-forward NN, which is used to fit the two-body and three-body terms in this PES. In order to take account of computational efficiency and fitting precision, a series of tests have been taken to determine the structures of the NNs.

The two-body potential energies ($V_{\text{HH}}^{(2)}$ and $V_{\text{LiH}}^{(2)}$) were fitted based on the energy points obtained at the MRCI/CBS level. For two-body potential energies, the NNs include two hidden layers and there are five neurons in each hidden layer. The precision of the fitting was very high and the RMSEs are extremely small (1.0×10^{-7} eV for $V_{\text{HH}}^{(2)}$ and 3.6×10^{-7} eV for $V_{\text{LiH}}^{(2)}$).

For the PES, the three-body term is the critical factor that determines the quality of the PES. In order to improve the precision and save the consumption of computing power, the hierarchical construction (HC) scheme⁴³ was used to construct the three-body term $V_{\text{LiHH}}^{(3)}(\mathbf{R})$. In the HC method, a high-accuracy PES can be structured by summing a low-accuracy PES and a different PES for high- and low-accuracy *ab initio* methods. The low-accuracy PES is fitted based on dense *ab initio* points, and the different PES is fitted based on sparse *ab initio* points. In this work, the three-body term $V_{\text{LiHH}}^{(3)}(\mathbf{R})$ at the MRCI/CBS level can be expressed as

$$V_{\text{LiHH}}^{(3)}(\mathbf{R}) = V_{\text{QZ}}^{(3)}(\mathbf{R}) + \Delta V_{\text{CBS-QZ}}^{(3)}(\mathbf{R}), \quad (6)$$

where $V_{\text{QZ}}^{(3)}(\mathbf{R})$ is fitted based on 12156 *ab initio* MRCI/(WCVQZ_{Li}/AVQZ_H) three-body points, and $\Delta V_{\text{CBS-QZ}}^{(3)}$ is fitted based on 2234 difference values between three-body potential energies at the MRCI/CBS and MRCI/(WCVQZ_{Li}/AVQZ_H) levels. $V_{\text{QZ}}^{(3)}(\mathbf{R})$ and $\Delta V_{\text{CBS-QZ}}^{(3)}$ were fitted by the NN method, and two hidden layers (11 neurons in the first hidden layer, 12 neurons in the second hidden layer) were included in the NNs. To solve the problem of adaptation of permutation symmetry in three-body potential energies, low-order permutation invariant polynomials (PIPs)^{44,45} were used as inputs for the NNs.

By summing the two-body potential energies and the three-body term as in eqn (3), a high-accuracy PES V_{total} was obtained with the RMSE only 0.004 eV.

2.3 Features of the LiH₂ potential energy surface

Table 1 shows the spectroscopic constants of LiH($X^1\Sigma^+$) and H₂($X^1\Sigma_g^+$) obtained from the new PES, as compared with the

Table 1 The spectroscopic constants for LiH($X^1\Sigma^+$) and H₂($X^1\Sigma_g^+$) obtained from the new PES, compared with the experimental data^{46,47} and results obtained on the Wernli PES and the Prudente PES^{17,18}

		Expt.	This work	Prudente PES	Wernli PES
H ₂ ($X^1\Sigma_g^+$)	R_e (Å)	0.7414	0.7414	0.7416	0.7420
	D_e (cm ⁻¹)	38288.0	38313.2	38181.5	38521.0
	ω_e (cm ⁻¹)	4401.21	4411.77	—	4463.55
	$\omega_e x_e$ (cm ⁻¹)	121.33	124.44	—	124.87
LiH($X^1\Sigma^+$)	R_e (Å)	1.5956	1.5957	1.6075	1.6081
	D_e (cm ⁻¹)	20288.7	20296.3	20092.3	19968.0
	ω_e (cm ⁻¹)	1405.65	1402.56	—	1297.58
	$\omega_e x_e$ (cm ⁻¹)	23.20	23.05	—	21.71

experimental data.^{46,47} The theoretical results obtained from the other two PESs^{17,18} are also listed in the table. It can be found that our results agree very well with the experimental data, which indicates that the new PES gives a good description of the two-body potential energy. The fitted bond lengths of LiH and H₂ are almost the same as the experimental data. The bond energies are slightly higher than the experimental results (25.2 cm⁻¹ for H₂ and 7.6 cm⁻¹ for LiH). The calculated frequency and anharmonicity constant are close to the experimental data. Fig. 1 shows the topographical features of the three-dimensional ground PES at four different Li–H–H angles (180°, 135°, 90°, and 45°). The PESs are smooth over the whole configuration space. There are two valleys in each of the four surfaces: the left valley and right valley correspond to the product of Li + H₂ and reactant of H + LiH, respectively. The left one is deeper than the right one because the reaction of H + LiH → Li + H₂ is exothermic. Fig. 2 shows the minimum energy paths (MEPs) from LiH to H₂ at four different approaching angles. It clearly shows that there is no obvious barrier or well along the pathway, which is similar to the PES obtained by Wernli *et al.*¹⁷ This implies that no threshold exists in the reaction of H(2S) + LiH($X^1\Sigma^+$) → Li(2S) + H₂($X^1\Sigma_g^+$). The exothermicity for the title reaction is 2.235 eV. The zero-point energy of the reactant LiH is 0.086 eV, and the zero-point energy of the product H₂ is 0.272 eV. So the exothermicity is 2.049 eV when the zero-point energies are taken into account. Fig. 3(a) shows a color plot of the potential energy for a Li atom moving around a H₂ diatom with the bond length fixed at the equilibrium distance (0.7414 Å), which lies along the *x*-axis with the center of the bond fixed at the origin. In the plot, the energy is set as zero when the atom is far away from the diatom. As seen in the figure, there is no well or barrier, and the Li atom is always repulsed by the H₂ molecule wherever the Li atom is. Similarly, Fig. 3(b) shows a plot of the potential energy when the H atom moves around the LiH diatom with the bond length fixed at its equilibrium geometry (1.5957 Å). There exists a deep well around the fixed H atom. When the H atom gets into the region of the well with low collision energy, it tends to be attracted by the fixed H atom. We conclude that the well plays an important role in the reaction of H(2S) + LiH($X^1\Sigma^+$) → Li(2S) + H₂($X^1\Sigma_g^+$), particularly at low collision energy.

3 Dynamical calculations

On this new PES, the dynamics of the H(2S) + LiH($X^1\Sigma^+$) → Li(2S) + H₂($X^1\Sigma_g^+$) reaction were investigated using the TDWP method, which has been applied widely in many reactive systems.^{30,48–52} Detailed discussions on the TDWP method can be found in relevant literature,^{49,53} and here we give a brief introduction. The reactant Jacobi coordinates are applied in the body-fixed representation, and the Hamiltonian can be written as

$$\hat{H} = -\frac{\hbar^2}{2\mu_R} \frac{\partial^2}{\partial R^2} - \frac{\hbar^2}{2\mu_r} \frac{\partial^2}{\partial r^2} + \frac{(\hat{J} - \hat{j})^2}{2\mu_R R^2} + \frac{\hat{j}^2}{2\mu_r r^2} + \hat{V}, \quad (7)$$

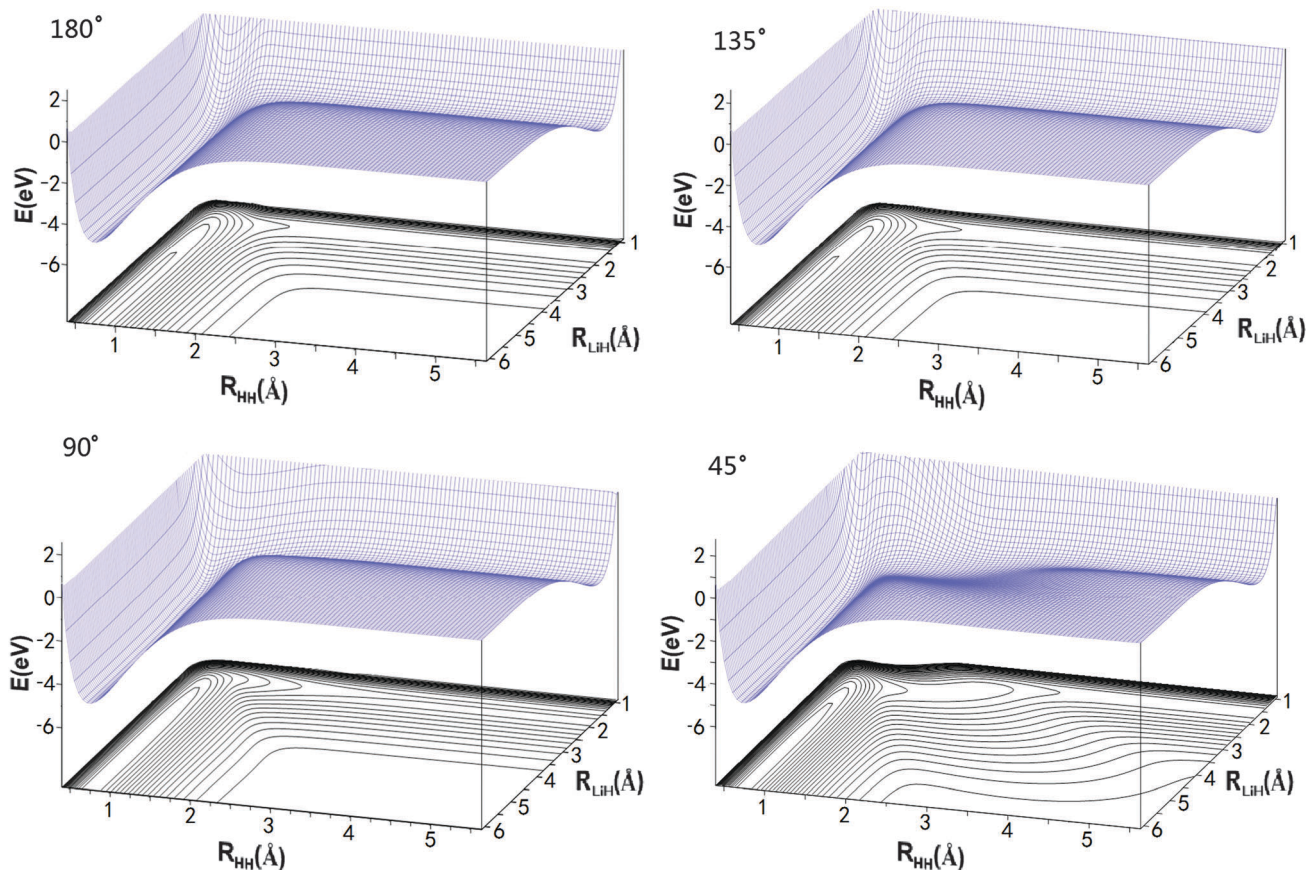


Fig. 1 Potential energy surfaces for the four Li–H–H angles 180°, 135°, 90° and 45°.

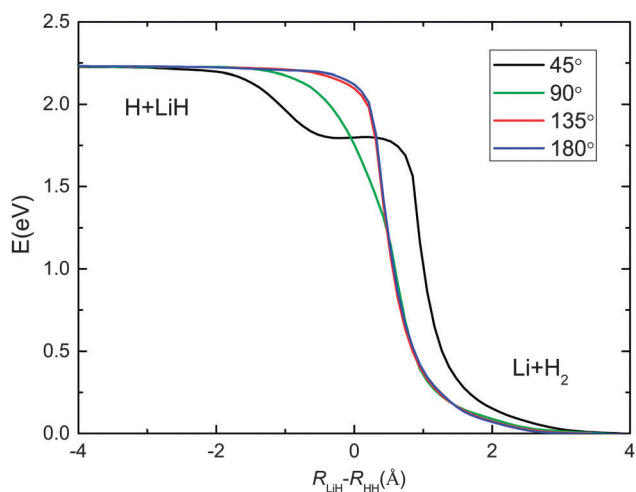


Fig. 2 Minimum energy paths for the new PES at four Li–H–H angles.

where R is the distance from the H atom to the mass center of the LiH molecule, and r is the bond length of the LiH molecule. μ_R and μ_r are the corresponding reduced masses associated with the R and r coordinates. \hat{J} and \hat{j} are the angular momentum operators of the LiH₂ system and the reactant diatomic molecule. \hat{V} represents the potential energy of the LiH₂ system. The state-to-state S -matrix $S_{vjK \leftarrow v_0j_0K_0}^J(E)$ is extracted using the

reactant coordinate-based method.⁵⁴ The state-to-state reaction probability is calculated by

$$P_{vj \leftarrow v_0j_0}^J = \frac{1}{2j_0 + 1} \sum_{K, K_0} |S_{vjK \leftarrow v_0j_0K_0}^J|^2. \quad (8)$$

The state-to-state integral cross sections (ICSS) and differential cross sections (DCSS) are obtained by

$$\sigma_{vj \leftarrow v_0j_0} = \frac{\pi}{(2j_0 + 1)k_{v_0j_0}^2} \sum_K \sum_{K_0} \sum_J (2J + 1) |S_{vjK \leftarrow v_0j_0K_0}^J|^2 \quad (9)$$

and

$$\frac{d\sigma_{vj \leftarrow v_0j_0}(\theta, E)}{d\Omega} = \frac{1}{(2j_0 + 1)} \sum_K \sum_{K_0} \left| \frac{1}{2ik_{v_0j_0}} \sum_J (2J + 1) d_{KK_0}^J(\theta) S_{vjK \leftarrow v_0j_0K_0}^J \right|^2, \quad (10)$$

where θ is the scattering angle. The rovibrational state of the reactant molecule LiH is set as $v_0 = 0, j_0 = 0$. In the TDWP method, the parameters determined through numerous tests are listed in Table 2.

Fig. 4 shows the total reaction probabilities of the $\text{H}(^2\text{S}) + \text{LiH}(X^1\Sigma^+) \rightarrow \text{Li}(^2\text{S}) + \text{H}_2(X^1\Sigma_g^+)$ reaction with different total angular momentum quantum numbers as a function of collision energy.

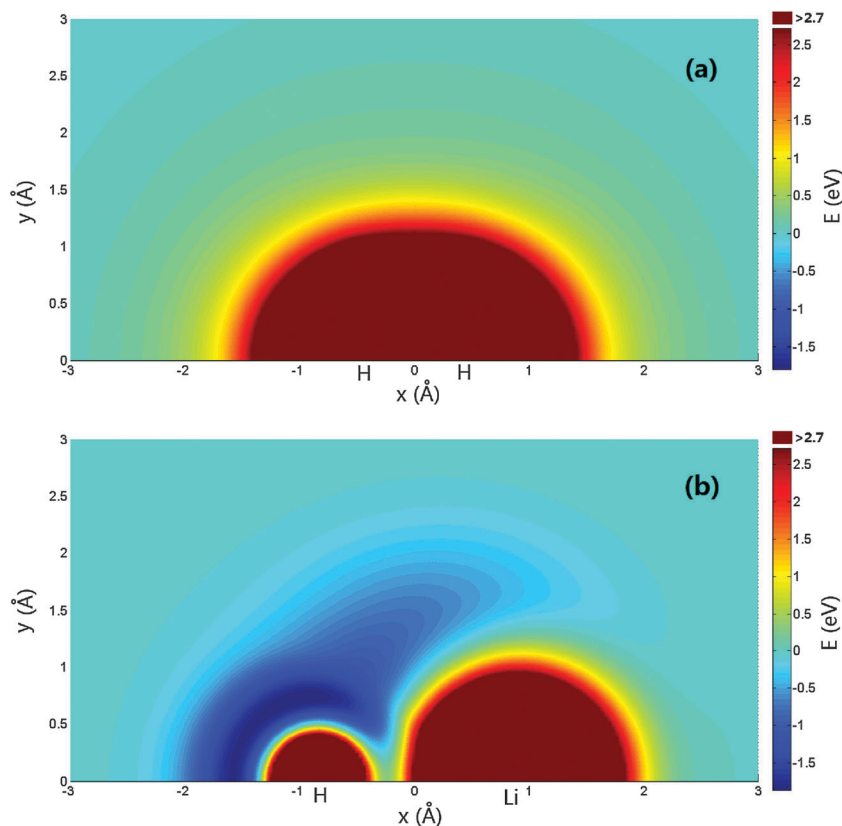


Fig. 3 (a) Color plot of the potential energy when the Li atom moves around the H₂ diatom with the bond length fixed at $R_{\text{HH}} = 0.7414 \text{ \AA}$ (this lies along the x -axis with the center of the bond fixed at the origin). (b) Color plot of the potential energy when the H atom moves around the HLi diatom with the bond length fixed at $R_{\text{HLi}} = 1.5957 \text{ \AA}$.

For the case of total angular momentum quantum number $J = 0$, there is no threshold in the reaction probability. This implies that the reaction is spontaneous. As the J value increases, the threshold appears due to the emergence of the centrifugal barrier. There exists a mass of the resonance structures on the reaction probability curves, which is an important signal of the quantum effect. Similar features have also been reported in previous work.^{18,27,28} Padmanaban *et al.* have studied^{19,21} resonance structures, and they found the resonance structures correspond to the metastable vibrational levels of the LiH₂ system.²¹ As the collision energy increases, the resonance structures become

Table 2 Numerical parameters used in the TDWP calculations (atomic units are used)

H(² S) + LiH(X ¹ Σ ⁺) → Li(² S) + H ₂ (X ¹ Σ _g ⁺)	
Grid/basis range and size	$R \in [0.01, 25.0]$, $N_R = 199$ $r \in [0.01, 20.0]$, $N_r = 149$ $N_j = 199$
Initial wave packet	$R_c = 16.5$ $\Delta_R = 0.25$ $k_0 = \sqrt{2E_0\mu_R}$ with $E_0 = 0.5 \text{ eV}$
Total propagation time	30 000 iterations
Highest J value	53

less pronounced because the reactive collisions become more direct. For comparison purposes, the reaction probabilities obtained on the Prudente PES¹⁸ and the Wernli PES¹⁷ using the TDWP method are also shown in Fig. 4. The applied numerical parameters are the same as those in the TDWP calculations on the present PES. The reaction probabilities calculated on the Prudente PES¹⁸ are significantly different from the other two results, because on this PES there exists an early-staged energy barrier.²⁹ A similar early-staged energy barrier was not found on the present PES or the Wernli PES.¹⁷ The results obtained on the present PES and the Wernli PES¹⁷ are similar at most of the collision energies, but show significant differences at very low collision energy. This can be explained by the fact that the calculated result of reaction dynamics is sensitive to the PES at low collision energy. The reaction probabilities obtained on the present PES are higher at very low collision energy, thus it is easier for the system to react at low temperatures.

In the TDWP calculation, the maximal total angular momentum quantum number is $J = 53$, and its threshold is slightly higher than 0.5 eV, which is the upper collision energy limit in the calculation of the ICS. The total ICS of the H(²S) + LiH(X¹Σ⁺) → Li(²S) + H₂(X¹Σ_g⁺) reaction as a function of collision energy is shown in Fig. 5. As shown in the figure, no threshold exists due to the absence of an energy barrier on the minimum energy path. At low collision energy, the ICS value is

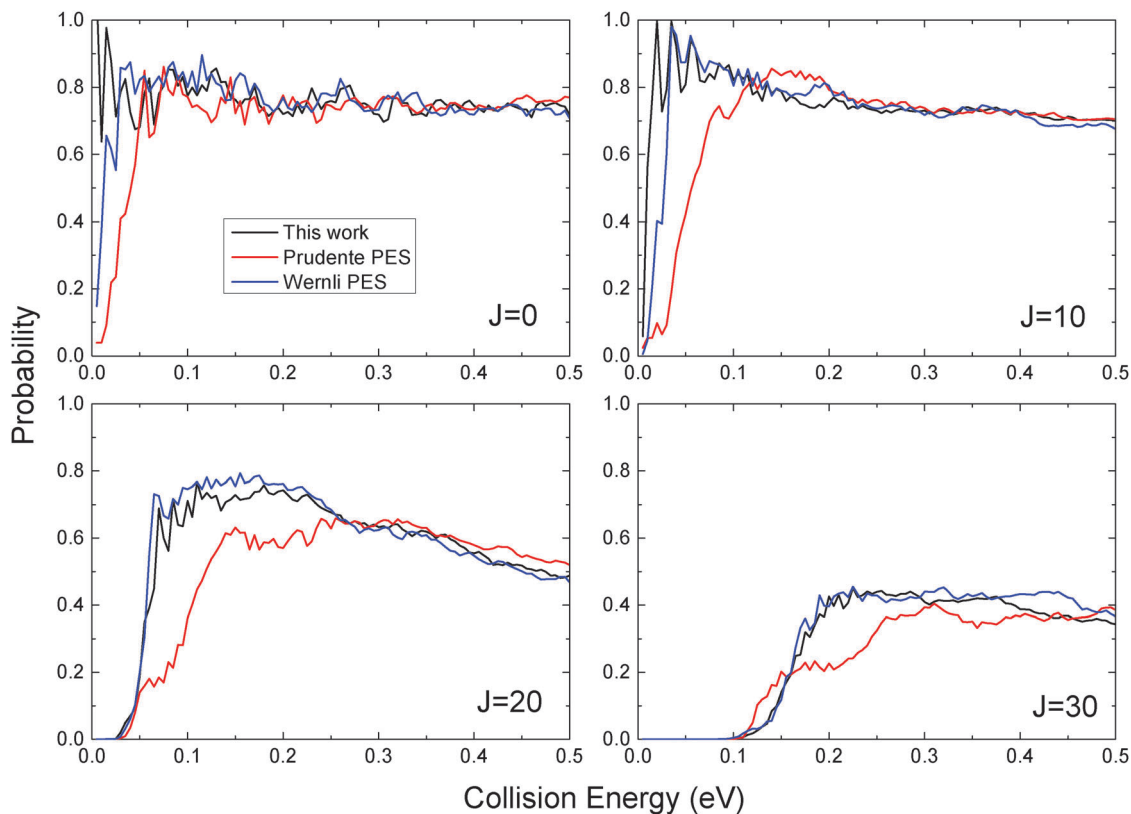


Fig. 4 Total reaction probabilities of the $\text{H}(^2\text{S}) + \text{LiH}(X^1\Sigma^+) \rightarrow \text{Li}(^2\text{S}) + \text{H}_2(X^1\Sigma_g^+)$ reaction calculated by the TDWP method using the present PES, the Prudente PES [ref. 18] and the Wernli PES [ref. 17].

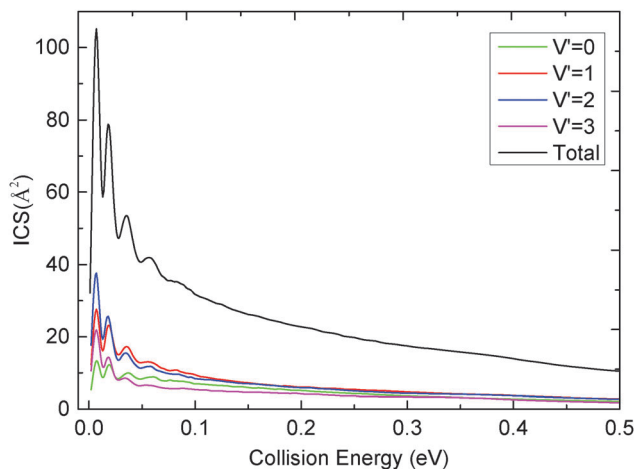


Fig. 5 Total and vibrationally resolved ICSs of the $\text{H}(^2\text{S}) + \text{LiH}(X^1\Sigma^+) \rightarrow \text{Li}(^2\text{S}) + \text{H}_2(X^1\Sigma_g^+)$ reaction calculated by the TDWP method.

high, and it decreases with increasing collision energy. This can be explained by the features of the PES. At low collision energy, the H atom moves towards the LiH molecule slowly, and the H atom will be attracted to another H atom when it gets into the region of the well mentioned in Fig. 3(b). The LiH_2 system has enough time to adjust to produce the H_2 molecule. However, as the collision energy increases, the time for adjustment gets shorter, which leads to the decrease in ICS. At low collision

energy, several peaks can be found on the ICS resulting from the resonance effect. To get information on the vibrational states of the product H_2 molecule, the ICSs of the first four vibrational states ($\nu' = 0$ to 3) are also presented in the figure. The ICS values of $\nu' = 1$ and 2 are larger than those of $\nu' = 0$ and 3, because the exothermicity is large enough to vibrationally excite the product H_2 molecule.

Fig. 6 shows the total ICS compared with the results obtained on the Wernli PES¹⁷ and the Prudente PES¹⁸ using the TDWP method. The ICS obtained on the Prudente PES¹⁸ is lower than the other two results, which can be attributed to the early-staged energy barrier. At high collision energy, all the ICSs decrease with increasing collision energy, and our result is almost the same as that obtained on the Wernli PES.¹⁷ At low collision energy, compared with the ICS obtained on the Wernli PES,¹⁷ our result is significantly higher and the resonance peaks are more obvious. This again illustrates the importance of PES accuracy to reaction dynamics at low collision energy, because a small difference in the PES might lead to a significant difference in reaction dynamics.

To study the angular distribution of the product, DCSs at three collision energies (0.1 eV, 0.3 eV and 0.5 eV) were calculated and are shown in Fig. 7. The DCS results indicate that the product molecule tends to be forward scattering. For the $\text{H}(^2\text{S}) + \text{LiH}(X^1\Sigma^+) \rightarrow \text{Li}(^2\text{S}) + \text{H}_2(X^1\Sigma_g^+)$ reaction, no potential well exists on the minimum energy path, so most reactive collisions are direct collisions. Therefore, the system

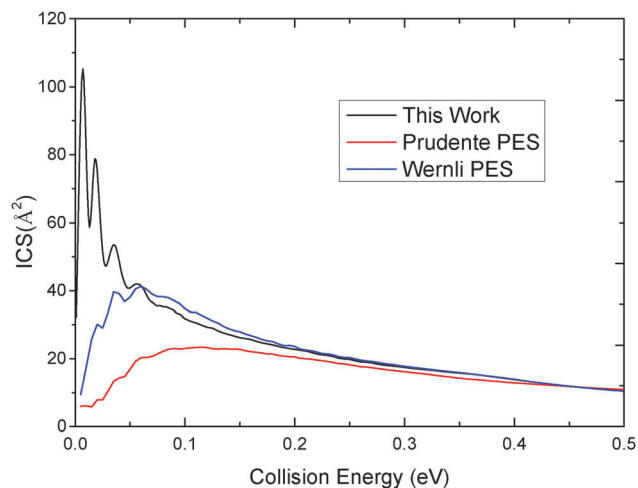


Fig. 6 Total ICSs of the $\text{H}(^2\text{S}) + \text{LiH}(X^1\Sigma^+) \rightarrow \text{Li}(^2\text{S}) + \text{H}_2(X^1\Sigma_g^+)$ reaction calculated by the TDWP method on the present PES, the Prudente PES [ref. 18] and the Wernli PES [ref. 17].

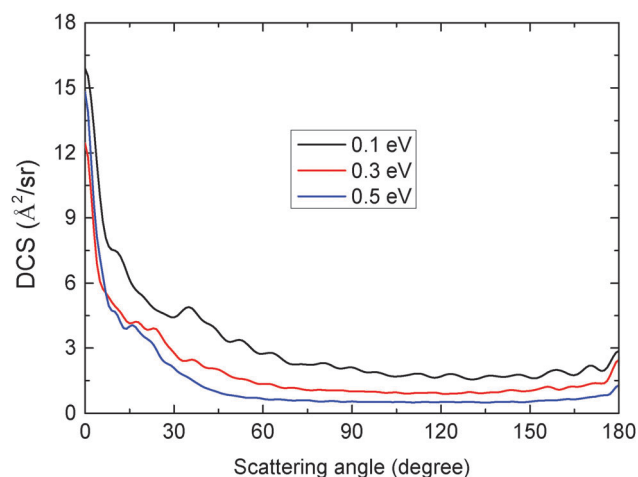


Fig. 7 DCSs of the $\text{H}(^2\text{S}) + \text{LiH}(X^1\Sigma^+) \rightarrow \text{Li}(^2\text{S}) + \text{H}_2(X^1\Sigma_g^+)$ reaction at three collision energies (0.1 eV, 0.3 eV and 0.5 eV).

doesn't have enough time to wash away the initial memory of the reactant. This leads to an obvious bias in the angular distribution of the product H_2 molecule. With the collision energy increasing, the trend of forward scattering becomes more apparent because the reactive collisions become more direct.

4 Conclusion

In this work, we have reported a new PES of the ground electronic state of the LiH_2 system based on high-level energies. The *ab initio* energies were calculated at the MRCI level with aug-cc-pVXZ ($X = \text{Q}, 5$) basis sets and the energies at the CBS limit were obtained using these *ab initio* energies. The NN method was used to structure both the two-body and three-body potential energy terms, and the HC scheme was used to construct the three-body term. The RMSE of the fitting result is only 0.004 eV. The spectroscopic constants for $\text{LiH}(X^1\Sigma^+)$ and

$\text{H}_2(X^1\Sigma_g^+)$ obtained from the new PES agree very well with the experimental data. The calculation of TDWP was carried out for the $\text{H}(^2\text{S}) + \text{LiH}(X^1\Sigma^+) \rightarrow \text{Li}(^2\text{S}) + \text{H}_2(X^1\Sigma_g^+)$ reaction on the new PES. The reaction probabilities, ICSs and DCSs of the title reaction were calculated. The reaction probability curves show a mass of resonance structures corresponding to the metastable vibrational levels of the LiH_2 system. The resonance structures become less prominent with increasing collision energy, because the reaction prefers direct collisions. No threshold exists in the reaction due to the absence of the energy barrier on the minimum energy path. At low collision energy, the ICS value is high, and this decreases with increasing collision energy. At low collision energy, there are several peaks on the total ICS curve, which is a typical characteristic of the resonance. The ICS values of $\nu' = 1$ and 2 are larger than those of $\nu' = 0$ and 3, because the exothermicity is large enough to vibrationally excite the product H_2 molecule. The DCS results indicate that the product molecule tends to be forward scattering due to the direct reactive collisions. With increasing collision energy, the tendency of forward scattering becomes more pronounced because the reactive collisions are more direct.

Acknowledgements

This work was supported by the National Natural Science Foundation of China (Grant No. 11374045), the Fundamental Research Funds for the Central Universities (Grant No. DUT13ZD207), and Program for New Century Excellent Talents in University (Grant No. NCET-12-0077).

References

- 1 D. Galli and F. Palla, *Astron. Astrophys.*, 1998, **335**, 403.
- 2 M. Signore, G. Vedrenne, P. Debernardis, V. Dubrovich, P. Encrenaz, R. Maoli, S. Masi, G. Mastrantonio, B. Melchiorri, F. Melchiorri and P. E. Tanzilli, *Astrophys. J. Suppl.*, 1994, **92**, 535.
- 3 R. Maoli, F. Melchiorri and D. Tosti, *Astrophys. J.*, 1994, **425**, 372.
- 4 P. C. Stancil and A. Dalgarno, *Astrophys. J.*, 1997, **479**, 543.
- 5 P. C. Stancil, S. Lepp and A. Dalgarno, *Astrophys. J.*, 1996, **458**, 401.
- 6 V. K. Dubrovich and A. A. Lipovka, *Astron. Astrophys.*, 1995, **296**, 301.
- 7 S. Lepp and J. M. Shull, *Astrophys. J.*, 1984, **280**, 465.
- 8 S. Lepp, P. C. Stancil and A. Dalgarno, *J. Phys. B: At., Mol. Opt. Phys.*, 2002, **35**, R57.
- 9 E. Bodo, F. A. Gianturco and R. Martinazzo, *Phys. Rep.*, 2003, **384**, 85.
- 10 L. J. Dunne, J. N. Murrell and P. Jemmer, *Chem. Phys. Lett.*, 2001, **336**, 1.
- 11 N. J. Clarke, M. Sironi, M. Raimondi, S. Kumar, F. A. Gianturco, E. Buonomo and D. L. Cooper, *Chem. Phys.*, 1998, **233**, 9.
- 12 H. S. Lee, Y. S. Lee and G. H. Jeung, *J. Phys. Chem. A*, 1999, **103**, 11080.

- 13 K. H. Kim, Y. S. Lee, T. Ishida and G. H. Jeung, *J. Chem. Phys.*, 2003, **119**, 4689.
- 14 H. Berriche, *THEOCHEM*, 2004, **682**, 89.
- 15 H. Berriche and C. Tlili, *THEOCHEM*, 2004, **678**, 11.
- 16 E. Bodo, F. A. Gianturco, R. Martinazzo and M. Raimondi, *Eur. Phys. J. D*, 2001, **15**, 321.
- 17 M. Wernli, D. Caruso, E. Bodo and F. A. Gianturco, *J. Phys. Chem. A*, 2009, **113**, 1121.
- 18 F. V. Prudente, J. M. C. Marques and A. M. Maniero, *Chem. Phys. Lett.*, 2009, **474**, 18.
- 19 R. Padmanaban and S. Mahapatra, *J. Theor. Comput. Chem.*, 2006, **5**, 871.
- 20 R. Padmanaban and S. Mahapatra, *J. Phys. Chem. A*, 2006, **110**, 6039.
- 21 R. Padmanaban and S. Mahapatra, *J. Chem. Phys.*, 2002, **117**, 6469.
- 22 P. Defazio, C. Petrongolo, P. Gamallo and M. Gonzalez, *J. Chem. Phys.*, 2005, **122**, 214303.
- 23 K. C. Lin and R. Vetter, *Int. Rev. Phys. Chem.*, 2002, **21**, 357.
- 24 T. Roy, T. R. Rao and S. Mahapatra, *Chem. Phys. Lett.*, 2011, **501**, 252.
- 25 S. Gomez-Carrasco, L. Gonzalez-Sanchez, N. Bulut, O. Roncero, L. Banares and J. F. Castillo, *Astrophys. J.*, 2014, **784**, 55.
- 26 M. Hsiao, K. Lin and Y. Hung, *J. Chem. Phys.*, 2011, **134**, 034119.
- 27 T. Roy and S. Mahapatra, *J. Chem. Phys.*, 2012, **136**, 174313.
- 28 R. Padmanaban and S. Mahapatra, *J. Chem. Phys.*, 2004, **121**, 7681.
- 29 G. Sha, J. Yuan, C. Meng and M. Chen, *Chem. Res. Chin. Univ.*, 2013, **29**, 956.
- 30 Y. Li, J. Yuan, M. Chen, F. Ma and M. Sun, *J. Comput. Chem.*, 2013, **34**, 1686.
- 31 Y. Q. Li, F. C. Ma and M. T. Sun, *J. Chem. Phys.*, 2013, **139**, 154305.
- 32 Y. Q. Li, Y. Z. Song, P. Song, Y. Z. Li, Y. Ding, M. T. Sun and F. C. Ma, *J. Chem. Phys.*, 2012, **136**, 194705.
- 33 C. M. Handley and P. L. A. Popelier, *J. Phys. Chem. A*, 2010, **114**, 3371.
- 34 J. Behler, *Phys. Chem. Chem. Phys.*, 2011, **13**, 17930.
- 35 T. Wang, J. Chen, T. Yang, C. Xiao, Z. Sun, L. Huang, D. Dai, X. Yang and D. H. Zhang, *Science*, 2013, **342**, 1499.
- 36 H. J. Werner and P. J. Knowles, *J. Chem. Phys.*, 1988, **89**, 5803.
- 37 P. J. Knowles and H. J. Werner, *Chem. Phys. Lett.*, 1988, **145**, 514.
- 38 H. J. Werner and P. J. Knowles, *J. Chem. Phys.*, 1985, **82**, 5053.
- 39 P. J. Knowles and H. J. Werner, *Chem. Phys. Lett.*, 1985, **115**, 259.
- 40 MOLPRO: <http://www.molpro.net/>.
- 41 D. G. Truhlar, *Chem. Phys. Lett.*, 1998, **294**, 45.
- 42 H. Rabitz and O. F. Alis, *J. Math. Chem.*, 1999, **25**, 197.
- 43 B. Fu, X. Xu and D. H. Zhang, *J. Chem. Phys.*, 2008, **129**, 011103.
- 44 B. Jiang and H. Guo, *J. Chem. Phys.*, 2013, **139**, 054112.
- 45 B. J. Braams and J. M. Bowman, *Int. Rev. Phys. Chem.*, 2009, **28**, 577.
- 46 K. P. Huber and G. Herzberg, *Constants of diatomic molecules*, Springer, 1979.
- 47 W. C. Stwalley and W. T. Zemke, *J. Phys. Chem. Ref. Data*, 1993, **22**, 87.
- 48 Z. Sun, L. Liu, S. Y. Lin, R. Schinke, H. Guo and D. H. Zhang, *Proc. Natl. Acad. Sci. U. S. A.*, 2010, **107**, 555.
- 49 Z. Sun, S. Y. Lee, H. Guo and D. H. Zhang, *J. Chem. Phys.*, 2009, **130**, 174102.
- 50 Z. Sun, W. Yang and D. H. Zhang, *Phys. Chem. Chem. Phys.*, 2012, **14**, 1827.
- 51 D. Cheng, J. Yuan and M. Chen, *J. Phys. Chem. A*, 2014, **118**, 55.
- 52 J. Yuan, D. Cheng and M. Chen, *RSC Adv.*, 2014, **4**, 36189.
- 53 Z. Sun, H. Guo and D. H. Zhang, *J. Chem. Phys.*, 2010, **132**, 084112.
- 54 Z. Sun, X. Lin, S. Y. Lee and D. H. Zhang, *J. Phys. Chem. A*, 2009, **113**, 4145.